American Mineralogist, Volume 97, pages 1060–1069, 2012

Minerals in cement chemistry: A single-crystal neutron diffraction and Raman spectroscopic study of thaumasite, $Ca_3Si(OH)_6(CO_3)(SO_4)\cdot 12H_2O$

G. Diego Gatta,[1,2,*] Garry J. McIntyre,[3] Julia G. Swanson,[4] and Steven D. Jacobsen[4]

[1]Dipartimento di Scienze della Terra, Universita' degli Studi di Milano, Via Botticelli 23, I-20133 Milano, Italy
[2]CNR-Istituto per la Dinamica dei Processi Ambientali, Milano, Italy
[3]The Bragg Institute, Australian Nuclear Science and Technology Organisation, Locked Bag 2001, Kirrawee DC, New South Wales 2232, Australia
[4]Department of Earth and Planetary Sciences, Northwestern University, Evanston, Illinois 60208, U.S.A.

Abstract

Thaumasite, $Ca_3Si(OH)_6(CO_3)(SO_4)\cdot 12H_2O$, is recognized as a secondary-alteration mineral and indicator of sulfate attack in Portland cement in contact with sulfate-rich groundwater, especially in cold regions. The hydrogen positions in thaumasite have been determined from single-crystal neutron diffraction structure refinements at 300 and 22 K. No phase transitions occur within the temperature range investigated. The structure of thaumasite is largely held together by hydrogen bonding. The major structural units [CO_3 groups, SO_4 tetrahedra, $Si(OH)_6$ octahedra, and $Ca(OH)_4(H_2O)_4$ polyhedra] are interconnected via 10 distinct hydrogen bonds. Analysis of the difference-Fourier maps of the nuclear density reveals the positions of all 10 hydrogen atoms in the structure, and the hydrogen bonding becomes shorter (stronger) upon decreasing temperature to 22 K. The SO_4 tetrahedron expands upon decreasing temperature (i.e., negative thermal expansion at the molecular level), driven by shortening of the hydrogen bonding between $[Ca_3Si(OH)_6(H_2O)_{12}]^{4+}$ columns. Polarized Raman spectra of thaumasite show that the ν_1 symmetric stretching modes of $Si(OH)_6$, SO_4, and CO_3 occur at 658, 983, and 1066 cm^{-1}, respectively. In addition, the out-of-plane bending mode (ν_2) and asymmetric stretching mode (ν_3) of the carbonate group are tentatively assigned to bands at 887 and 1400 cm^{-1}, respectively. Bands at 418 and 455 cm^{-1} (and possibly at 477 cm^{-1}) are attributed to the symmetric bending modes (ν_2) of the sulfate group, and we observe a possible asymmetric stretching mode (ν_3) of SO_4 at 1090–1100 cm^{-1}. Splitting of some sulfate and carbonate vibrational modes may occur due to hydrogen bonding on all the oxygen sites. At 1685–1710 cm^{-1} we observe the H_2O bending modes (H-O-H), and from 2900–3600 cm^{-1} there are 13 distinct bands associated with bending overtones and the O-H stretching vibrations corresponding to H-positions determined in the neutron diffraction study. The effect of the low-temperature stability of thaumasite on the pronounced "thaumasite sulfate attack" of Portland cements observed in cold regions is discussed.

Keywords: Thaumasite, Portland cements, crystal chemistry, single-crystal neutron diffraction, Raman spectroscopy, hydrogen bonding

Introduction

Thaumasite, $Ca_3Si(OH)_6(CO_3)(SO_4)\cdot 12H_2O$ [a ~11.030, c ~10.396 Å, space group $P6_3$, $Z = 2$], occurs as a low-temperature secondary-alteration phase in mafic igneous and metamorphic rocks. Usually it is associated with zeolites, apophyllite, analcime, calcite, gypsum, and pyrite. Thaumasite forms a solid solution with ettringite, $Ca_6[Al(OH)_6]_2(SO_4)_3\cdot 26H_2O$ (Moore and Taylor 1970; Barnett et al. 2000), and contains a highly unusual Si site in six-coordination with hydroxyl, ^{VI}Si-OH.

Thaumasite and ettringite also form in the porous matrix of aging concrete, especially in contact with sulfate-rich soils or fluids (Crammond 1985) or when limestone is used as a filling material (Hartshorn et al. 1999). Cement hydration products, calcium silicate hydrates—the so-called C-S-H and calcium hydroxide—portlandite $Ca(OH)_2$, are decomposed as a result of both sulfate attack and of carbonation. Because C-S-H in concrete provides most of the binding strength, thaumasite and ettringite formation leads to weakening and disintegration of the cement matrix especially in concrete structures below ground (e.g., Hartshorn et al. 1999; Bensted 1999; Hobbs and Taylor 2000; Santhanam et al. 2001; Zhang et al. 2009). Degradation of concrete by thaumasite sulfate attack (TSA) has been documented in various environments including an 80-year-old aqueduct in Manitoba, 33-year-old pavement in Ontario, test samples exposed to marine (tidal) conditions, and in laboratory samples exposed to wet–dry cycles in sulfate solution (Thomas et al. 2003). The source of carbonate differs in each of these cases, deriving from de-dolomitization of dolostone aggregates, carbonate ions in the seawater, or atmospheric CO_2 through the process of carbonation. Sulfate attack of Portland cement by thaumasite appears to be greatly accelerated at sub-zero temperatures, as observed from rapid deterioration of reinforced concrete foundations in the Arctic within just two years of construction (Bickley 1999).

The crystal chemistry of thaumasite is unusual: it contains

* E-mail: diego.gatta@unimi.it

0003-004X/12/0007–1060$05.00/DOI: http://dx.doi.org/10.2138/am.2012.4058

about 42 wt% H_2O, 7 wt% CO_2, 13 wt% SO_3, 28 wt% CaO, and 10 wt% SiO_2, giving a density of only ~1.88 g/cm^3. The crystal structure of thaumasite was solved by Edge and Taylor (1971), and later refined by Zemann and Zobetz (1981), Effenberger et al. (1983), and Jacobsen et al. (2003) by single-crystal X-ray diffraction. The thaumasite structure consists of $[Ca_3Si(OH)_6(H_2O)_{12}]^{4+}$ columns running parallel to [001], connected by CO_3^{2-} and SO_4^{2-} groups via hydrogen bonds with H_2O molecules, as shown in Figures 1 and 2. Thaumasite is the only mineral containing silicon in six-coordination with hydroxyl $(OH)^-$ that is stable at low *P-T* conditions. High pressure favors six-coordination of Si with oxygen, such as in stishovite (SiO_2) and silicate perovskite ($MgSiO_3$), but the high-pressure synthetic phase D ($MgSi_2H_2O_6$) is the only other phase known to contain ^{VI}Si-OH (Yang et al. 1997; Frost and Fei 1998).

The thermal behavior of thaumasite has been investigated by in situ single-crystal X-ray structure refinements at 130 and 298 K by Jacobsen et al. (2003), and no phase transitions were observed over this temperature range. The unit cell and CaO_8 polyhedra showed significant positive thermal expansion over the temperature range investigated (130–298 K), but the silicate octahedron, sulfate tetrahedron, and the carbonate group show zero or negative thermal expansion. Jacobsen et al. (2003) suggested that there is an important role played by the hydrogen bonds on this unusual thermal behavior, but clarification of this role is obscured by the difficulties in defining the hydrogen-bond geometry (i.e., O-H and H···O distances and O-H···O angle) from X-ray data.

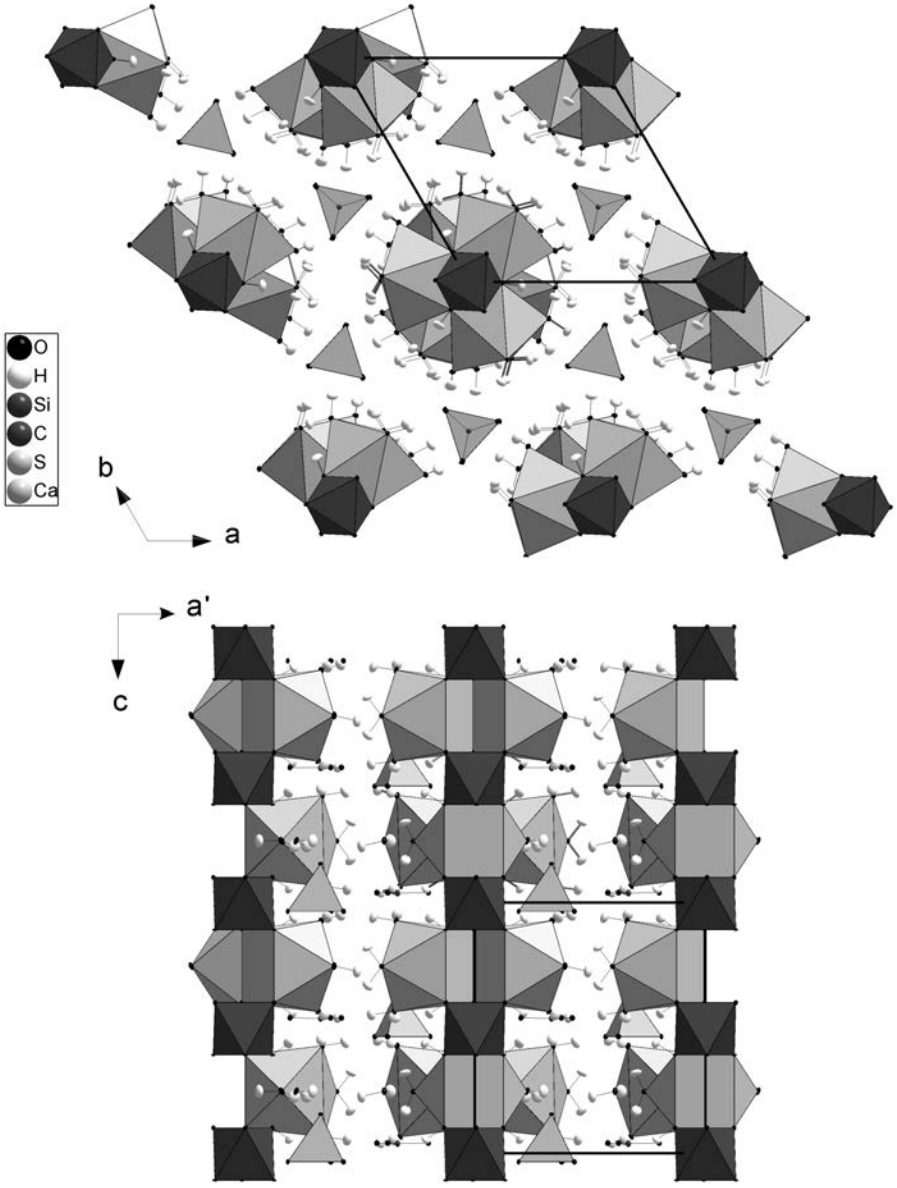

Figure 1. The crystal structure of thaumasite viewed down [001] and [010] based on the neutron structure refinement at 22.5 K of this study. Thermal-ellipsoid probability factor: 50%.

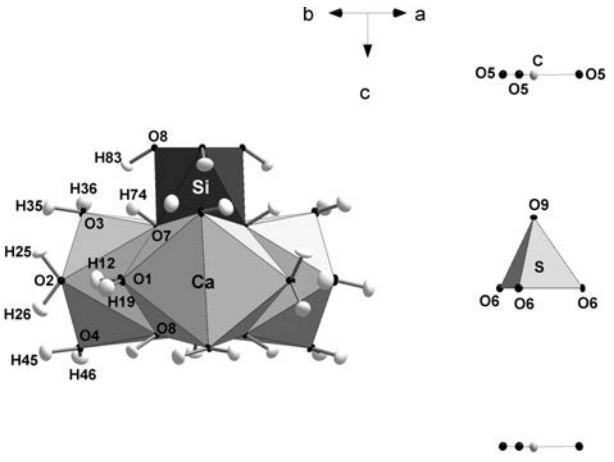

FIGURE 2. Configuration of the $[Ca_3Si(OH)_6(H_2O)_{12}]$ building-block units forming columns parallel to [001] (**left side**), and of the alternating CO_3 groups and SO_4 tetrahedra running along [001] (**right side**), based on the neutron structure refinement at 22.5 K of this study. Thermal-ellipsoid probability factor: 50%.

The results of high-temperature synchrotron powder diffraction between 303 and 1098 K, and of TG/TDA up to 1073 K, were reported by Martucci and Cruciani (2006). Rietveld refinements showed no phase transition up to 417 K, whereupon thaumasite decomposed. A continuous dehydration process was observed between 303–393 K, whereas at $T > 393$ the dehydration was severe, leading to a collapse of the structure at $T \geq 417$ K. The dehydration-induced amorphization was confirmed by the TG/DTA analyses, which shows a slower weight loss at $T < 353$ K and a very rapid weight loss (~43 wt%) in the temperature range between 393 and 453 K. This behavior suggests that the stability of thaumasite is mainly governed by the crystal-lattice H_2O, highlighting the importance of determining the hydrogen-bonding environment in thaumasite.

Raman spectroscopy has become an important tool for quickly identifying the formation of thaumasite in concrete and for distinguishing thaumasite from ettringite in field samples. Brough and Atkinson (2001) reported Raman spectra of thaumasite as well as the long-term stability of thaumasite at up to 373 K from those spectra. Sahu et al. (2002) used a Raman chemical imaging technique to refine methods further for distinguishing thaumasite from ettringite, which is not considered as detrimental to concrete as thaumasite. Polarized Raman spectra of thaumasite single crystals showing the full details of vibrational modes in the structure have not been reported, nor have deconvolutions of the Raman spectra of thaumasite in the OH region been carried out.

Previous structure refinements of thaumasite at ambient and non-ambient conditions have been performed on the basis of X-ray diffraction data. This has led to a poorly defined picture of the configuration of the OH groups (e.g., with O-H distances at room temperature ranging between 0.65 and 1.25 Å; Effenberger et al. 1983, Jacobsen et al. 2003) and of the H-bonding. On this basis, the aim of the present study is to determine the hydrogen positions and hydrogen-bonding geometry of a natural thaumasite at ambient conditions and at low temperature (~22 K) by single-crystal neutron diffraction. We report reliable locations of all the proton sites and topological configuration of the hydrogen bonds, the anisotropic displacement parameters of the H sites, and discuss the role played by the H bonds on the low-temperature thermal behavior of thaumasite. Because we report the hydrogen-bonding environments in thaumasite with neutron diffraction techniques, new polarized Raman spectra, especially in the region of O-H stretching, are presented to complement the neutron study.

EXPERIMENTAL METHODS

Sample characterization

A natural, transparent, and eudedral (hexagonal prism) centimetric crystal of thaumasite from Black Rock Mine, Kuruman, Kalahari, Northen Cape Province, South Africa, was obtained from the National Museum of Natural History, Smithsonian Institution (NMNH no. 165279). The single crystal was cut into four sections for microprobe, thermo-gravimetric, Raman spectroscopy, and single-crystal neutron diffraction experiments.

Qualitative electron-probe X-ray microanalyses in the energy-dispersive mode (EDS-EPMA) and quantitative microanalyses in the wavelength-dispersive mode (WDS-EPMA) were performed on a polished single crystal of thaumasite using a JEOL JXA-8200 electron microprobe. The system was operated using a defocused electron beam to avoid dehydration and cation migration under the electron beam, following a protocol usually adopted for zeolite analysis (Gatta and Boffa Ballaran 2004). The preliminary EDS-EPMA analysis showed that only the elements nominally expected in thaumasite (i.e., Ca, Si, S) occurred within the detection limit. A series of natural minerals (K-feldspar for Si, wollastonite for Ca, barite for S) were used as standards for the WDS-EPMA analysis. The results were corrected for matrix effects using a conventional ZAF routine in the JEOL suite of programs. The average composition (30 point analysis) of thaumasite is: CaO 27.1(8) wt%, SiO_2 9.5(3) wt%, and SO_3 12.7(6) wt%. The crystal was chemically homogeneous within analytical errors. Thermo-gravimetric analyses (TG) were performed with a NETZSCH STA449C thermoanalyzer under a 20 mL/min air flux with a heating rate of 5 K/min, using a powdered sample (crystallite diameter 2–5 μm) previously dried at 310 K for 4 h. The experiment was conducted up to 1073 K. The weight loss was about 49.8% within the T-range investigated, which appears to reflect the theoretical amount of H_2O and CO_2 expected in thaumasite (i.e., ~43.4 wt% for H_2O, ~7.1 wt% CO_2). The WDS-EPMA and TG analyses, assuming an expected stoichiometric amount of H_2O and CO_2, confirm the ideal formula of thaumasite previously reported: $Ca_3Si(OH)_6(CO_3)(SO_4)\cdot 12H_2O$.

Raman spectroscopy

Raman spectra were collected using a 458 nm solid-state diode source laser with an output of 200 mW, operating with about 40 mW at the sample. Confocal and polarized Raman spectra were obtained using a customized Olympus BX microscope and 20× objective with an Andor Shamrock 303i spectrograph (1200 lines per mm grating) and a Newton DU-970-UVB electron multiplying CCD camera. Spectra were recorded using a 10 s exposure time, with three accumulations. Deconvolution of the Raman spectra in the O-H region was carried out using the program PeakFit Version 4.12.

Neutron diffraction

Neutron diffraction data were collected from a large euhedral fragment of the sample measuring about 39 mm^3 in volume at 301.0 and 22.5 K on the four-circle diffractometer D9 at the Institut Laue-Langevin, Grenoble, in a beam of wavelength 0.8381(2) Å obtained by reflection from a Cu(220) monochromator (Table 1). D9 is equipped with a small two-dimensional area detector (Lehmann et al. 1989), which for this measurement allowed observation of the centroids of all scanned reflections as well as optimal delineation of the peak from the considerable incoherent background due to the high hydrogen content. Nearly complete sets of unique reflections to 0.844/0.873 $Å^{-1}$ in $\sin\theta/\lambda$ were scanned at 301.0/22.5 K, as well as limited sets of equivalent reflections at lower $\sin\theta/\lambda$ to confirm the space group. For all data, background corrections following Wilkinson et al. (1988) and Lorentz corrections were applied. Absorption corrections were made by Gaussian integration (Coppens et al. 1965) using the calculated attenuation coefficient $\mu = 0.1023$ mm^{-1}, to give transmission ranges of 0.550–0.809 at both temperatures. Initial structural refinements with SHELX-97 (Sheldrick 2007) showed that extinction was quite

TABLE 1. Details of neutron data collection and refinement of thaumasite at 301.0 and 22.5 K

T (K)	301.0	22.5
Crystal shape	Hexagonal prism	Hexagonal prism
Crystal volume (mm^3)	39	39
Crystal color	Translucent white	Translucent white
Unit-cell constants	a = 11.0545(5) Å	a = 11.0360(5) Å
	c = 10.4131(6) Å	c = 10.3845(6) Å
Chemical formula	$Ca_3Si(OH)_6(CO_3)(SO_4)\cdot 12H_2O$	$Ca_3Si(OH)_6(CO_3)(SO_4)\cdot 12H_2O$
Space group	$P6_3$	$P6_3$
Z	2	2
Radiation type	neutron	neutron
Wavelength (Å)	0.8381(2)	0.8381(2)
Diffractometer	D9 four circle	D9 four circle
Data-collection method	ω–θ scans	ω–θ scans
Max. 2θ (°)	89.85	88.99
	$-4 \le h \le 14$	$-5 \le h \le 15$
	$-14 \le k \le 11$	$-15 \le k \le 12$
	$-14 \le l \le 17$	$-16 \le l \le 17$
No. measured reflections	2512	2825
No. unique reflections	1575	1937
No. unique refl. with $F_o > 4\sigma(F_o)$	1440	1830
No. refined parameters	184	183
R_{int}	0.0360	0.0329
R_1 (F) with $F_o > 4\sigma(F_o)$	0.0964	0.0701
R_1 (F) for all the unique reflections	0.1082	0.0765
wR_2 (F^2)	0.1045	0.0846
GooF	1.806	1.757
Weighting scheme: a, b	0.010, 0	0.010, 0
Residuals (fm/Å^3)	–1.1/+1.1	–1.8/+1.6

Notes: $R_{int} = \Sigma|F^2_{obs} - F^2_{obs}(\text{mean})|/\Sigma[F^2_{obs}]$, $R_1 = \Sigma(||F_{obs}| - |F_{calc}||)/\Sigma|F_{obs}|$. $wR_2 = \{\Sigma[w(F^2_{obs} - F^2_{calc})^2]/\Sigma[w(F^2_{obs})^2]\}^{0.5}$, $w = 1/[\sigma^2(F^2_{obs}) + (a\cdot P)^2 + b\cdot P]$. $P = [\text{Max}(F^2_{obs}, 0) + 2\cdot F^2_{calc}]/3$.

severe, but could be reasonably well accounted for by the Larson-like correction (extinction coefficient: ~0.01, Larson 1967). After corrections, the discrepancy factors among the symmetry-related reflections were R_{int} = 0.0360 and 0.0329 (Laue class 6/m) at 301.0 and 22.5 K, respectively. Least-squares matching of the observed and calculated centroids of the 381 strongest reflections at 301.0 K gave the unit-cell constants: a = 11.0545(5) and c = 10.4131(6) Å; the 563 strongest reflections at 22.5 K gave: a = 11.0360(5) and c = 10.3845(6) Å. Other details of the data collections are listed in Table 1.

Structure refinement

Intensity data of thaumasite collected at 301.0 K were first processed with the program E-STATISTICS, implemented in the WinGX package (Farrugia 1999). The Wilson plot, the normalized structure factors (E's) and their statistics of distributions, and Sheldrick's $|E^2 - 1|$ criterion (Sheldrick 2007) suggested that the structure of thaumasite is acentric. A valuable check on the supposed symmetry was obtained by comparing the equivalent reflections with the program ASSIGN-SPACEGROUP (in WinGX, Farrugia 1999), which selected the space group $P6_3$. The anisotropic crystal structure refinement was then performed in the space group $P6_3$ using the SHELX-97 software (Sheldrick 2007), starting from the atomic coordinates of Jacobsen et al. (2003), without any H sites. The neutron scattering lengths of Ca, Si, C, S, O, and H were used according to Sears (1986). Secondary isotropic extinction effects were corrected according to Larson's formalism (1967), as implemented in the SHELXL-97 package (Sheldrick 2007). When convergence was achieved, a series of intense negative residual peaks were found in the difference-Fourier synthesis of the nuclear density. Further cycles of refinement were then performed assigning H to these residual peaks, as hydrogen has a negative neutron scattering length. Convergence was rapidly achieved and the final least-square cycles were conducted with anisotropic thermal parameters for all the H sites. All the principal mean-square atomic displacement parameters were positively defined. The variance-covariance matrix showed no significant correlation among the refined parameters. At the end of the last cycle of refinement, no peak larger than –1.1/+1.1 fm/Å^3 was present in the final difference-Fourier map of the nuclear density (Table 1). The final agreement index (R_1) was 0.0964 for 184 refined parameters and 1440 unique reflections with $F_o > 4\sigma(F_o)$ (Table 1). Refined atomic coordinates and displacement parameters are reported in Tables 2, 3, and 4a. Relevant bond lengths and angles are listed in Table 5. A full list of bond distances and angles is given in Table 6[1].

The intensity data collected at 22.5 K were processed following the same strategy already adopted for the data set collected at 301.0 K. Anisotropic structure refinement was performed starting from the atomic coordinates from the structure model refined at 301.0 K. Convergence was rapidly achieved and the variance-covariance matrix showed no significant correlation among the refined parameters. No peak larger than –1.8/+1.6 fm/Å^3 was present in the difference-Fourier map of the nuclear density at the end of the last refinement cycle (Table 1). The final agreement index (R_1) was 0.0701 for 183 refined parameters and 1830 unique reflections with $F_o > 4\sigma(F_o)$ (Table 1). Atomic positions and displacement parameters are reported in Tables 2, 3, and 4b. Bond lengths and angles are given in Tables 5 and 6[1].

RESULTS AND DISCUSSION

The EMPA-EDS, EMPA-WDS, and TG analyses confirm the crystal chemistry of thaumasite obtained in the previous studies, and deliver further evidence about the almost ideal composition of the thaumasite from Kalahari, South Africa (Grubessi et al. 1986).

Neutron structure refinements based on the data collected at 301.0 and 22.5 K confirm the general structure model previously obtained (Edge and Taylor 1971; Zemann and Zobetz 1981; Effenberger et al. 1983; Jacobsen et al. 2003; Martucci and Cruciani 2006), showing that the symmetry of the thaumasite structure is maintained within the temperature range investigated, without any evidence of phase transitions. The diffraction data collected at only two temperatures does not allow a reliable description of the thermo-elastic behavior. However, within the precision and the accuracy of our unit-cell constants, we observe a thermo-elastic anisotropy, with the structure being more expandable along [001] than on (001) (α_a:α_c = 1:1.65), as observed by Jacobsen et al. (2003, between 130 and 298 K).

As pointed out by Jacobsen et al. (2003), all nine crystallographically unique oxygen sites in the thaumasite structure are involved in hydrogen bonding. O1, O2, O3, and O4 are H_2O-

[1] Deposit item AM-12-058, Table 6 and CIFs. Deposit items are available two ways: For a paper copy contact the Business Office of the Mineralogical Society of America (see inside front cover of recent issue) for price information. For an electronic copy visit the MSA web site at http://www.minsocam.org, go to the *American Mineralogist* Contents, find the table of contents for the specific volume/issue wanted, and then click on the deposit link there.

TABLE 2. Refined fractional atomic coordinates and equivalent/isotropic temperature factors (Å²), based on the diffraction data collected at 301.0 and 22.5 K

T (K)	301.0				22.5			
	x	*y*	*z*	U_{eq}/U_{iso}	*x*	*y*	*z*	U_{eq}/U_{iso}
Ca	0.1951(2)	0.9885(2)	0.2528(5)	0.0087(4)	0.19374(13)	0.98693(12)	0.25460(25)	0.0030(2)
Si	0	0	0.0054(8)	0.0044(6)	0	0	0.0042(5)	0.0011(3)
C	1/3	2/3	0.4643(5)	0.0161(7)	1/3	2/3	0.4617(2)	0.0062(3)
S	1/3	2/3	0.9846(8)	0.094(14)	1/3	2/3	0.9855(4)	0.0011
O1	0.3916(2)	0.2286(2)	0.2544(6)	0.0258(5)	0.39149(11)	0.22717(11)	0.25305(25)	0.0073(2)
O2	0.2616(2)	0.4030(2)	0.2541(5)	0.0207(4)	0.26355(11)	0.40223(11)	0.25438(22)	0.0062(2)
O3	0.0026(4)	0.3410(4)	0.0743(4)	0.0204(7)	0.00415(14)	0.33972(15)	0.07188(16)	0.0055(2)
O4	0.0240(3)	0.3471(4)	0.4342(3)	0.0161(6)	0.02555(14)	0.34834(15)	0.43514(14)	0.0047(2)
O5	0.2012(3)	0.6230(4)	0.4606(4)	0.0199(7)	0.20084(14)	0.62403(15)	0.45997(15)	0.0057(2)
O6	0.1926(3)	0.6239(4)	0.0340(3)	0.0200(7)	0.19079(14)	0.62274(16)	0.03458(14)	0.0047(2)
O7	0.1304(3)	0.1254(3)	0.1073(2)	0.0069(5)	0.13196(14)	0.12510(15)	0.10833(12)	0.0031(2)
O8	0.1308(3)	0.1243(3)	0.3991(2)	0.0094(5)	0.13134(15)	0.12444(15)	0.39906(13)	0.0038(2)
O9	1/3	2/3	0.8468(5)	0.0018(1)	1/3	2/3	0.8443(2)	0.0039(3)
H74	0.2137(6)	0.1938(7)	0.0616(7)	0.027(1)	0.2153(3)	0.1933(4)	0.0611(3)	0.0185(6)
H83	0.2096(6)	0.1960(7)	0.4442(5)	0.022(1)	0.2114(3)	0.1965(3)	0.4445(3)	0.0162(6)
H12	0.3663(5)	0.3000(5)	0.2532(13)	0.039(1)	0.3651(3)	0.2984(3)	0.2534(6)	0.0222(5)
H19	0.4885(5)	0.2706(6)	0.2751(7)	0.039(2)	0.4903(3)	0.2715(3)	0.2742(3)	0.0224(7)
H25	0.3008(8)	0.4660(7)	0.1793(6)	0.028(1)	0.3018(4)	0.4642(3)	0.1801(3)	0.0191(7)
H26	0.2963(9)	0.4625(8)	0.3288(9)	0.039(2)	0.2992(4)	0.4633(4)	0.3305(4)	0.0203(7)
H35	0.0731(7)	0.4351(7)	0.0578(8)	0.032(1)	0.0760(3)	0.4371(3)	0.0578(4)	0.0202(7)
H36	–0.0853(8)	0.3364(8)	0.0493(8)	0.035(1)	–0.0823(3)	0.3361(4)	0.0482(4)	0.0212(7)
H45	0.0994(6)	0.4478(7)	0.4456(8)	0.032(1)	0.0986(3)	0.4477(3)	0.4469(4)	0.0189(6)
H46	–0.0621(6)	0.3489(8)	0.4562(8)	0.030(1)	–0.0619(3)	0.3470(4)	0.4575(4)	0.0200(6)

Notes: U_{eq} is defined as one third of the trace of the orthogonalized U_{ij} tensor. Silicon refined isotropically at 301.0 K and sulfur refined isotropically at 22.5 K to avoid high correlation among the refined parameters, and then fixed in the last cycles of refinement.

TABLE 3. Refined displacement parameters (Å²) in the expression: $-2\pi^2[(ha^*)^2U_{11} + \ldots + 2hka^*b^*U_{12} + \ldots + 2klb^*c^*U_{23}]$, based on the data collected at 301.0 and 22.5 K

T (K)	301.0						22.5					
	U_{11}	U_{22}	U_{33}	U_{12}	U_{13}	U_{23}	U_{11}	U_{22}	U_{33}	U_{12}	U_{13}	U_{23}
Ca	0.0083(9)	0.0113(9)	0.0074(7)	0.0055(7)	–0.0023(2)	–0.004(2)	0.0036(4)	0.0038(4)	0.0019(4)	0.0021(3)	–0.0007(7)	–0.0009(7)
Si	–	–	–	–	–	–	0.0015(4)	0.0015(4)	0.0005(6)	0.0007(2)	0	0
C	0.012(1)	0.012(1)	0.025(2)	0.006(0)	0	0	0.0051(4)	0.0051(4)	0.0085(8)	0.0025(2)	0	0
S	0.012(2)	0.012(2)	0.005(3)	0.006(1)	0	0	–	–	–	–	–	–
O1	0.0135(9)	0.017(1)	0.042(1)	0.0040(8)	–0.007(2)	–0.004(2)	0.0046(3)	0.0051(3)	0.0111(4)	0.0015(3)	–0.0003(7)	–0.0030(7)
O2	0.022(1)	0.013(1)	0.022(1)	0.005(1)	0.000(2)	0.001(2)	0.0074(3)	0.0052(3)	0.0052(4)	0.0027(3)	0.0002(7)	–0.0003(6)
O3	0.017(1)	0.020(1)	0.028(2)	0.012(1)	–0.002(1)	0.008(1)	0.0036(4)	0.0043(4)	0.0078(5)	0.0014(3)	0.0010(4)	0.0020(4)
O4	0.011(1)	0.014(1)	0.020(1)	0.003(1)	0.000(1)	–0.008(1)	0.0034(4)	0.0043(4)	0.0055(5)	0.0013(3)	0.0014(4)	–0.0013(4)
O5	0.012(1)	0.017(1)	0.031(2)	0.008(1)	0.000(1)	–0.001(1)	0.0049(4)	0.0058(4)	0.0062(5)	0.0026(3)	–0.0004(4)	–0.0001(4)
O6	0.011(1)	0.023(2)	0.023(2)	0.006(1)	0.003(1)	0.001(1)	0.0024(4)	0.0056(5)	0.0059(5)	0.0018(4)	–0.0003(4)	0.0000(4)
O7	0.010(1)	0.009(1)	0.004(1)	0.006(1)	0.001(1)	–0.002(1)	0.0035(4)	0.0046(4)	0.0011(5)	0.0019(3)	–0.0002(4)	–0.0004(4)
O8	0.008(1)	0.006(1)	0.009(1)	0.000(1)	0.002(1)	–0.002(1)	0.0034(4)	0.0031(4)	0.0045(5)	0.0013(4)	0.0000(4)	0.0005(4)
O9	0.020(1)	0.020(1)	0.015(2)	0.010(1)	0	0	0.0046(5)	0.0046(5)	0.0025(7)	0.0023(2)	0	0
H74	0.014(2)	0.017(2)	0.039(4)	–0.001(2)	–0.002(2)	–0.001(2)	0.012(1)	0.017(1)	0.020(1)	0.002(1)	0.004(1)	0.002(1)
H83	0.023(3)	0.024(3)	0.013(2)	0.006(2)	–0.012(2)	–0.006(2)	0.013(1)	0.012(1)	0.016(1)	0.001(1)	–0.004(1)	–0.004(1)
H12	0.038(2)	0.029(2)	0.054(3)	0.019(2)	0.006(5)	0.001(5)	0.0235(9)	0.0164(8)	0.032(1)	0.0135(7)	–0.002(2)	–0.001(1)
H19	0.021(2)	0.039(3)	0.051(5)	0.011(2)	–0.008(2)	–0.003(3)	0.0120(9)	0.023(1)	0.028(2)	0.0057(8)	–0.001(1)	0.001(1)
H25	0.039(3)	0.029(3)	0.020(3)	0.020(3)	0.012(2)	0.004(2)	0.026(1)	0.018(1)	0.010(1)	0.009(1)	0.005(1)	0.006(1)
H26	0.038(4)	0.027(3)	0.040(4)	0.006(3)	0.011(3)	–0.006(3)	0.020(1)	0.019(1)	0.019(1)	0.008(1)	–0.001(1)	–0.008(1)
H35	0.026(3)	0.020(3)	0.047(4)	0.011(2)	0.001(3)	0.007(3)	0.019(1)	0.014(1)	0.025(2)	0.006(1)	0.004(1)	0.006(1)
H36	0.030(3)	0.034(3)	0.034(4)	0.011(3)	–0.003(3)	0.000(3)	0.018(1)	0.020(1)	0.026(2)	0.010(1)	–0.001(1)	0.003(1)
H45	0.014(2)	0.025(3)	0.039(3)	–0.003(2)	0.006(2)	–0.009(2)	0.013(1)	0.014(1)	0.024(2)	0.003(1)	0.002(1)	–0.001(1)
H45	0.020(2)	0.038(3)	0.039(4)	0.019(2)	0.005(2)	–0.008(3)	0.015(1)	0.026(1)	0.023(1)	0.013(1)	0.001(1)	–0.002(1)

Note: Silicon refined isotropically at 301.0 K and sulfur refined isotropically at 22.5 K to avoid high correlation among the refined parameters.

molecule oxygen atoms, belonging to the coordination shell of the Ca site (Fig. 2, Table 5). All the H_2O molecules are H bonded, with the following energetically favorable configurations: O1-H12···O2 (i.e., H_2O···H_2O interaction) and O1-H19···O9 (i.e., O9 belonging to a SO_4 group), O2-H25···O6 (i.e., O6 belonging to a SO_4 group) and O2-H26···O5 (i.e., O5 belonging to a CO_3 group), O3-H35···O6 and O3-H36···O5, O4-H45···O5, and O4-H46···O6 (Table 5). O7 and O8 are oxygen atoms of hydroxyl groups (i.e., O7-H74 and O8-H8, Fig. 2), and belong to the coordination shell of Ca and Si (Fig. 2, Table 5). The oxygen atoms of the hydroxyl groups act as donors forming H bonds with the H_2O oxygen sites as acceptors (i.e., O7-H74···O4 and O8-H83···O3, Table 5). All the H bonds show O···O distances <2.97 Å within the temperature range investigated (Table 5). All the building-block units of the thaumasite structure (i.e., CO_3 groups, SO_4 groups, $Si(OH)_6$ octahedra and $Ca(OH)_4(H_2O)_4$ polyhedra) are connected via H bonds.

The geometry of the H_2O molecule is now well defined: the O-H distances corrected for "riding motion" (Busing and Levy 1964) range between 0.970 and 1.031 Å at 301.0 K and 0.985–1.009 at 22.5 K (Table 5). The H-OW-H angles range between 102.8–108.6° at 301.0 K and between 103.7–108.0° at 22.5 K (Table 5). The unusually low (~103°, Table 5) or high (~109°, Table 5) H-OW-H angles are still in the range of the observed

TABLE 4a. Principal mean-square atomic displacements (U1, U2, and U3, $\times 10^4$ Å^2) and root-mean-square components (R1, R2, and R3, Å) based on the structural refinement at 301.0 K

Site	U1	U2	U3	R1	R2	R3	R1/R3
Ca	133(16)	77(19)	50(13)	0.115(7)	0.087(11)	0.071(9)	1.63
C	250(19)	117(15)	117(15)	0.158(6)	0.108(7)	0.108(7)	1.46
S	116(13)	116(37)	51(29)	0.107(6)	0.107(17)	0.071(20)	1.50
O1	440(16)	226(21)	108(10)	0.209(4)	0.150(7)	0.104(5)	2.02
O2	279(18)	220(10)	122(8)	0.166(5)	0.148(3)	0.110(4)	1.51
O3	345(19)	197(10)	71(29)	0.185(5)	0.140(4)	0.084(17)	2.20
O4	282(18)	120(17)	81(12)	0.167(5)	0.109(8)	0.090(7)	1.86
O5	314(18)	167(16)	115(19)	0.177(5)	0.129(6)	0.107(9)	1.65
O6	261(26)	237(16)	103(14)	0.161(8)	0.153(5)	0.101(7)	1.59
O7	107(9)	76(21)	24(15)	0.103(4)	0.087(12)	0.049(15)	2.11
O8	163(22)	75(15)	44(8)	0.127(9)	0.086(9)	0.066(6)	1.92
O9	199(20)	199(20)	155(18)	0.141(7)	0.141(7)	0.124(7)	1.13
H74	397(37)	328(49)	94(18)	0.199(9)	0.181(14)	0.096(9)	2.06
H83	355(49)	259(23)	45(24)	0.188(13)	0.160(7)	0.067(18)	2.80
H12	556(44)	366(37)	257(40)	0.235(9)	0.191(10)	0.160(12)	1.47
H19	535(52)	438(42)	193(21)	0.231(11)	0.209(10)	0.139(8)	1.66
H25	444(33)	249(53)	141(34)	0.210(8)	0.157(17)	0.118(14)	1.77
H26	662(71)	281(53)	240(27)	0.257(14)	0.167(16)	0.154(9)	1.66
H35	489(40)	274(41)	187(31)	0.221(9)	0.165(12)	0.136(11)	1.62
H36	430(67)	342(38)	273(26)	0.207(16)	0.185(10)	0.165(8)	1.25
H45	583(42)	272(42)	96(17)	0.241(9)	0.164(13)	0.097(9)	2.47
H46	483(41)	330(27)	88(49)	0.219(9)	0.181(7)	0.093(26)	2.34

TABLE 4b. Principal mean-square atomic displacements (U1, U2, and U3, $\times 10^4$ Å^2) and root-mean-square components (R1, R2, and R3, Å) based on the structural refinement at 22.5 K

Site	U1	U2	U3	R1	R2	R3	R1/R3
Ca	43(5)	33(8)	15(5)	0.066(4)	0.057(7)	0.039(6)	1.69
Si	15(6)	15(6)	5(6)	0.039(8)	0.039(8)	0.022(13)	1.73
C	85(8)	51(6)	51(6)	0.092(4)	0.071(5)	0.071(4)	1.29
O1	128(8)	55(8)	36(4)	0.113(4)	0.074(5)	0.060(3)	1.89
O2	81(6)	55(6)	49(7)	0.090(3)	0.074(4)	0.070(5)	1.29
O3	88(5)	47(9)	30(3)	0.094(3)	0.069(7)	0.055(3)	1.71
O4	80(7)	36(4)	24(6)	0.089(4)	0.060(3)	0.050(6)	1.83
O5	63(6)	59(6)	48(5)	0.079(4)	0.077(4)	0.069(4)	1.15
O6	61(7)	59(6)	23(5)	0.078(4)	0.077(4)	0.048(5)	1.63
O7	49(7)	35(4)	10(4)	0.070(5)	0.059(3)	0.032(6)	2.21
O8	47(6)	39(8)	29(4)	0.069(4)	0.062(6)	0.054(4)	1.27
O9	46(2)	46(8)	25(7)	0.068(1)	0.068(6)	0.050(7)	1.36
H74	260(22)	205(15)	90(10)	0.161(7)	0.143(5)	0.095(5)	1.70
H83	239(22)	178(12)	68(9)	0.155(7)	0.133(5)	0.082(5)	1.87
H12	316(12)	238(8)	113(16)	0.178(3)	0.154(3)	0.106(8)	1.67
H19	295(21)	257(18)	119(8)	0.172(6)	0.160(6)	0.109(4)	1.57
H25	295(23)	209(14)	69(12)	0.172(7)	0.145(5)	0.083(7)	2.07
H26	288(23)	202(14)	118(16)	0.170(7)	0.142(5)	0.109(7)	1.56
H35	277(15)	217(22)	110(11)	0.166(5)	0.147(7)	0.105(5)	1.59
H36	277(18)	195(9)	165(23)	0.166(5)	0.140(3)	0.129(9)	1.30
H45	260(18)	199(21)	109(7)	0.161(6)	0.141(7)	0.104(3)	1.54
H46	270(16)	221(15)	108(19)	0.164(5)	0.149(5)	0.104(9)	1.58

TABLE 5. Relevant bond distances (Å) and angles (°) based on the diffraction data collected at 301.0 and 22.5 K

T (K)	301.0		22.5	
Ca-O1	2.449(4)		2.451(2)	
Ca-O2	2.521(4)		2.516(2)	
Ca-O3	2.412(6)		2.430(3)	
Ca-O4	2.405(6)		2.400(3)	
Ca-O7	2.486(5)		2.477(3)	
Ca-O7	2.451(5)		2.455(3)	
Ca-O8	2.480(5)		2.464(3)	
Ca-O2	2.521(3)		2.516(2)	
<Ca-O>	2.466		2.464	
Si-O7 (×3)	1.769(6)		1.785(4)	
Si-O8 (×3)	1.794(6)		1.786(4)	
<Si-O>	1.782		1.785	
C-O5 (×3)	1.289(4)	1.2937*	1.293(2)	1.2935*
S-O6 (×3)	1.475(5)		1.486(3)	
S-O9	1.435(10)		1.465(5)	
<S-O>	1.465		1.481	
O1-H12	0.960(7)	0.9790*	0.965(4)	0.9853*
O1-H19	0.955(6)	0.9720*	0.972(3)	0.9910*
H12-O1-H19	108.6(6)		108.0(3)	
O1···O2	2.924(4)		2.908(2)	
H12···O2	1.988(7)		1.964(4)	
O1-H12···O2	164.3(5)		165.5(3)	
O1···O9	2.827(4)		2.817(2)	
H19···O9	1.885(6)		1.859(3)	
O1-H19···O9	168.5(6)		168.3(3)	
O2-H25	0.966(9)	0.9987*	0.976(4)	0.9946*
O2-H26	0.966(9)	0.9896*	0.984(4)	1.0019*
H25-O2-H26	105.7(8)		105.7(4)	
O2···O6	2.808(6)		2.799(2)	
H25···O6	1.823(7)		1.827(3)	
O2-H25···O6	174.2(6)		174.6(3)	
O2···O5	2.745(6)		2.724(2)	
H26···O5	1.781(9)		1.742(4)	
O2-H26···O5	174.4(8)		175.3(4)	
O3-H35	0.9531(7)	0.9703*	0.976(3)	0.9940*
O3-H36	0.982(10)	0.9921*	0.967(4)	0.9849*
H35-O3-H36	104.9(8)		104.4(4)	
O3···O6	2.793(5)		2.778(2)	
H35···O6	1.845(7)		1.807(3)	
O3-H35···O6	172.3(7)		172.5(3)	
O3···O5	2.744(6)		2.745(3)	
H36···O5	1.809(11)		1.822(5)	
O3-H36···O5	158.0(9)		158.6(5)	
O4-H45	1.010(7)	1.0309*	0.991(3)	1.0088*
O4-H46	0.990(9)	1.0127*	0.985(4)	1.0042*
H45-O4-H46	102.8(7)		103.7(4)	
O4···O5	2.691(5)		2.680(2)	
H45···O5	1.692(7)		1.698(3)	
O4-H45···O5	169.3(7)		169.7(3)	
O4···O6	2.772(6)		2.762(3)	
H46···O6	1.805(10)		1.804(5)	
O4-H46···O6	164.6(8)		163.6(4)	
O7-H74	0.975(6)	1.0014*	0.980(3)	1.0003*
O7···O4	2.921(4)		2.913(2)	
H74···O4	1.967(7)		1.952(3)	
O7-H74···O4	165.3(6)		166.2(3)	
O8-H83	0.957(6)	0.9757*	0.966(3)	0.9836*
O8···O3	2.972(4)		2.929(2)	
H83···O3	2.034(6)		1.984(3)	
O8-H83···O3	165.7(6)		165.4(3)	

* Bond distance corrected for "riding motion" following Busing and Levy (1964).

H-O-H angles in solid-state materials (Chiari and Ferraris 1982; Steiner 1998 and references therein; Gatta et al. 2008). With such configurations, all the hydrogen bonds tend to approach linearity (which is energetically less costly, Steiner 1998), as shown by all the O-H···O angles ≥160° (Table 5). For the hydroxyl groups, the O-H distances corrected for "riding motion" range between 0.976–1.001 Å at 301.0 K and 0.984–1.000 Å at 22.5 K (Table 5). The oxygen and hydrogen atoms of the H_2O molecules have larger anisotropic displacement parameters than those belonging to the OH groups at 301.0 and 22.5 K (Tables 4a and 4b).

Edge and Taylor (1971), Zemann and Zobetz (1981), and Effenberger et al. (1983) reported a significant deviation of the carbonate group from planarity, which was significantly larger in the structure model of Edge and Taylor (1971) [i.e., 0.15(3) Å, in the direction away from the apical oxygen O9 of the sulfate tetrahedron] than in Zemann and Zobetz (1981) and Effenberger et al. (1983) [i.e., 0.094(19) and 0.060(9) Å, respectively, but in the opposite direction: toward the apical oxygen of the sulfate tetrahedron]. Less pronounced is the aplanarity found by Jacobsen et al. (2003), especially at low temperature [i.e., 0.044(3) Å at 298 K and 0.026(5) Å at 130 K, in the direction toward the apical oxygen of sulfate]. Our data show a modest deviation from planarity according to the configuration observed by Zemann and Zobetz (1981), Effenberger et al. (1983), and Jacobsen et al. (2003) (i.e., toward the apical oxygen of the sulfate tetrahedron),

which tends to decrease at low temperature [i.e., 0.039(2) Å at 301.0 K and 0.018(1) Å at 22.5 K]. Such an aplanarity appears to be common in several carbonate minerals, where C usually lies ~0.02 Å above the oxygen plane (Reeder 1983). As pointed out by Jacobsen et al. (2003), the CO_3 group in thaumasite shows a slightly longer C-O bond distance, when compared to other CO_3-bearing compounds (average value: 1.284 ± 4 Å, Zemann 1981), with almost-zero thermal expansion between 130 and 298 K. We obtained C-O5 = 1.289(3) Å at 301.0 K (Table 5), which does not experience any contraction at low temperature [i.e., C-O5 = 1.293(1) at 22.5 K, Table 5]. Slightly longer C-O bond distances might reflect the strong H bond to O5, being O4···O5 = 2.691(5) Å at 301.0 K and O4···O5 = 2.680(2) Å at 22.5 K (Table 5). In addition, the O5 oxygen acts as acceptor for other H bonds, with O2 and O3 as donors (Table 5).

In the thaumasite structure, the SO_4 tetrahedron (Fig. 2) is significantly distorted, with $\Delta(S\text{-}O)_{max} \approx 0.040$ Å (i.e., the difference between the longest and the shortest bond distances) at 301.0 K (see Table 5). In agreement with the previous experimental results, also in this case we observe a negative thermal expansion of the SO_4 tetrahedron, as shown by the shortest (i.e., S-O9, –2.1% from 22.5 to 301.0 K) and the longest (i.e., S-O6, –0.75% from 22.5 to 301.0 K) bond distances (Table 5). The O6 site acts as acceptor for three different H bonds, with O2, O3, and O4 as donors. The O9 site acts as acceptor for only one H bond, with O1 as donor. Hydrogen bonds with O6 as acceptor appear to be stronger than that with O9, and such a configuration is maintained at low temperature (Table 5). However, at 22.5 K the H bonds to O6 and O9 are stronger than the respective ones at 301.0 K. On this basis, we cannot exclude that the negative thermal expansion of the SO_4 group is the result of the stronger H-bonding scheme at low temperature. Within the experimental errors, the O-S-O angles appear to be maintained within the temperature range investigated (Table 6), and so no significant deformation of the tetrahedron occurs.

Our data show that the $Si(OH)_6$ octahedron in the thaumasite structure (Fig. 2) experiences a low-temperature-induced "regularization," being $\Delta(Si\text{-}O)_{max} \approx 0.025$ Å at 301.0 K and $\Delta(Si\text{-}O)_{max} \approx 0.001$ Å at 22.5 K (Table 5). In addition, the two unique bond distances of the polyhedron show an opposite behavior at low temperature: Si-O7 shows a negative thermal expansion (–0.90%, from 22.5 to 301.0 K), whereas Si-O8 shows a positive thermal expansion (+0.44%, from 22.5 to 301.0 K). These results agree with the experimental finding of Jacobsen et al. (2003), who reported a zero or slightly negative thermal expansion of the $Si(OH)_6$ octahedron between 130 and 298 K.

The $Ca(OH)_4(H_2O)_4$ polyhedron (Fig. 2) shows a modest positive thermal expansion within the temperature range investigated (i.e., with <Ca-O> ~ 2.458 at 301.0 K and <Ca-O> ~ 2.456 Å at 22.5 K, Table 5), with no change in distortion [i.e., with $\Delta(Ca\text{-}O)_{max}$ ~ 0.116 Å at both 301.0 and 22.5 K, Table 5].

Raman spectra in the 0–1000 cm^{-1} region are shown in Figure 3, with the laser parallel to the [100] direction and polarized at various angles counterclockwise (ccw) to the [001] direction. Here we do not attempt to make band assignments to the low-wavenumber lattice modes at 90–250 cm^{-1}, but note their positions and variation of intensity with polarization to assist future studies of Raman spectra of cement materials. The first bands of mention occur at 418 and 455 cm^{-1} (as well as 477 cm^{-1}), which may be attributed to the ν_2 symmetric bending mode(s) of the sulfate tetrahedron. Splitting of the ν_2 mode has been reported in natural ettringite with bands at 416 and 449 cm^{-1} (Deb et al. 2003) and in the mineral thenardite, Na_2SO_4 (Renaudin et al. 2007). Splitting of the ν_2 band of SO_4 in thaumasite may be due to the two different hydrogen bonds on apical (O9) and basal (O6 × 3) oxygen. An additional band at 477 cm^{-1} is observed in some orientations, which may also be due to the ν_2 mode(s) of the SO_4 group (Fig. 3). Also in Figure 3 we observe a band at 588 cm^{-1}, which may be due to the ν_4 asymmetric bending mode of SO_4, and a band at 887 cm^{-1} possibly due to the ν_2 out-of-plane bending mode of the carbonate group. The dominant feature of the spectrum at 0–950 cm^{-1} (Fig. 3) is the 658 cm^{-1} band due to the ν_1 symmetric stretching band of the $^{VI}Si\text{-}(OH)_6$ group.

In Figure 4, we extend the Raman shift out to 1250 cm^{-1} and include a direction of the laser parallel to [001] for comparison with the spectra with the laser parallel to [100]. The dominant peaks occur at 658 cm^{-1} (ν_1 $SiOH_6$), 983 cm^{-1} (ν_1 SO_4), and 1066 cm^{-1} (ν_1 CO_3), which are the symmetric stretching modes (ν_1) of those groups. Variation of intensity with orientation of the ν_1 modes of the sulfate and carbonate groups is shown in Figure 5. Referring to Figure 6, a shoulder of the 1066 cm^{-1} ν_1 carbonate band at ~1090–1112 cm^{-1} is highly variable in intensity as one rotates the laser polarization about the [100] axis and could be due to the ν_3 asymmetric stretching mode of the SO_4 group. When the laser is parallel to [001], an additional band in this region at 1132 cm^{-1} is observed (Fig. 4). Figure 6 also shows a possible ν_3 asymmetric stretching mode of the carbonate group at 1400 cm^{-1} and the H_2O bending vibrations (H-O-H) at 1685–1710 cm^{-1}.

Figure 7 shows Raman spectra of thaumasite in the region

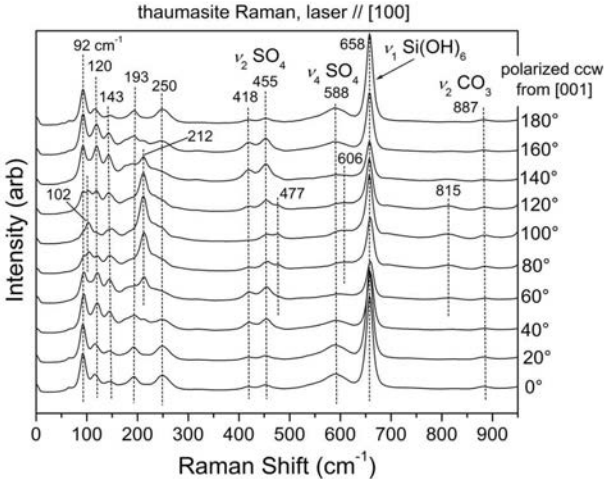

FIGURE 3. Raman spectra of thaumasite with the laser parallel to [100] and at various polarizations counterclockwise (ccw) from [001]. The symmetric bending mode of the SO_4 tetrahedron (ν_2) is tentatively assigned to 418 and 455 cm^{-1}, split possibly due to the two different hydrogen bonds on the sulfate group. An additional band at 477 cm^{-1} is observed at some orientations and may also be due to ν_2 of the SO_4 group. The band at 588 cm^{-1} may be assigned to the asymmetric bending mode (ν_4) of SO_4. Symmetric stretching of $Si\text{-}(OH)_6$ occurs at 658 cm^{-1}. The 887 cm^{-1} band may be due to the ν_2 out-of-plane bending mode of the carbonate group.

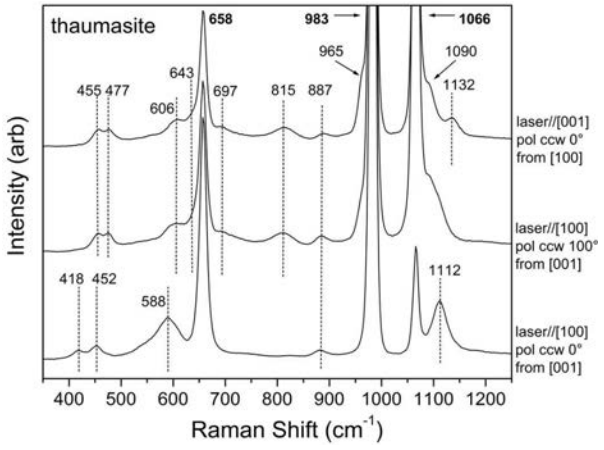

FIGURE 4. Raman spectra of thaumasite in the 350–1250 cm^{-1} range showing (in bold) positions of the ν_1 symmetric stretching modes of the $Si(OH)_6$, SO_4, and CO_3 groups at 658, 983, and 1066 cm^{-1}, respectively. Details reveal several bands at 418–477 cm^{-1} possibly associated with the ν_2 symmetric-bending mode of the SO_4 group, a band at 887 cm^{-1} possibly associated with the ν_2 out-of-plane CO_3 bending, as well as several bands at 1090–1132 cm^{-1} possibly associated with ν_3 asymmetric stretching modes of the SO_4 group.

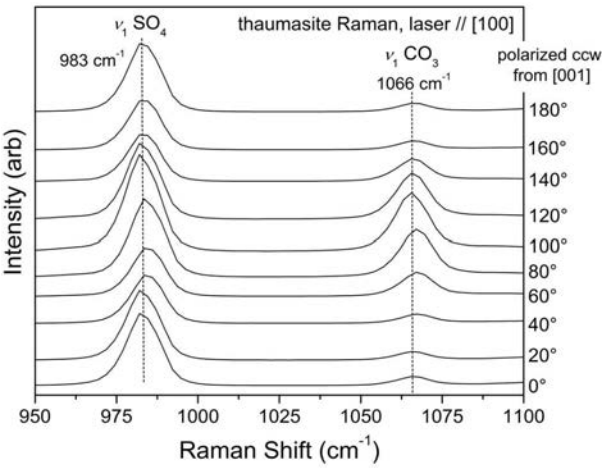

FIGURE 5. Polarized Raman spectra of thaumasite as a function of azimuth relative [001] with the laser along [100] showing variation of intensity of the fundamental ν_1 symmetric stretching mode of the CO_3 group. The ν_1 symmetric stretching mode of SO_4 occurs at 983 cm^{-1}.

of H_2O between 2500 and 3800 cm^{-1}. Spectra obtained with the laser parallel to [100] are identical to the spectra shown in Figure 7 polarized 100° from [001]. Therefore, Figure 7 depicts all of the possible observed bands in this region. To deconvolve the spectra, starting band positions were selected based on the dashed lines shown in Figure 7. From 2800–3300 cm^{-1} three broad peaks are identified, which display variation of intensity with orientation. In addition, six sharper peaks from 3300–3600 cm^{-1} are used to begin the fitting procedure of 13 total bands in the polarized spectra between 2800 and 3600 cm^{-1}.

Figure 8 shows the final fitted spectra for thaumasite in the H_2O region, which consists of at least 13 distinct bands associated

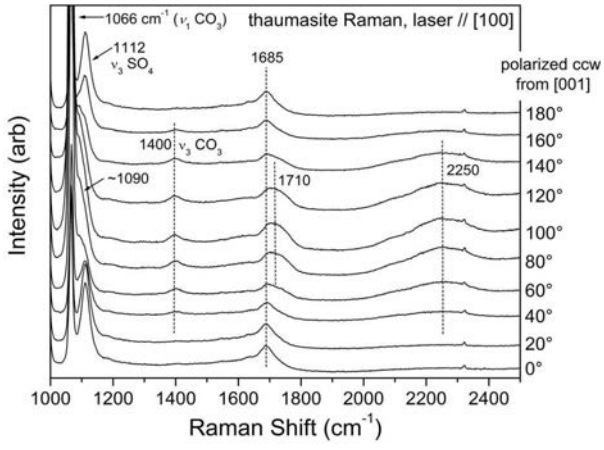

FIGURE 6. Polarized Raman spectra of thaumasite in the 1000–2500 cm^{-1} range showing variability in the 1090–1112 cm^{-1} bands, associated with the ν_3 asymmetric stretching mode of the SO_4 group. In addition, a 1400 cm^{-1} band possibly associated with ν_3 (asymmetric stretching) of CO_3 as well as H_2O bending vibrations (H-O-H) at 1685–1710 cm^{-1} are observed.

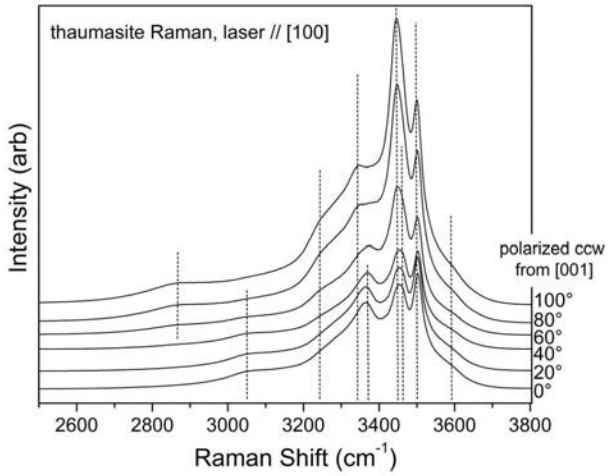

FIGURE 7. Polarized Raman spectra of thaumasite from 2500–3800 cm^{-1} showing variability of bands associated with O-H stretching and H-O-H bending overtones. Dashed lines represent starting positions for the deconvolution of the spectra in the H_2O region.

with O-H stretching and H-O-H bending overtones. At wavenumbers above 3200 cm^{-1}, we fitted 10 consistent peaks associated with O-H stretching in the thaumasite structure based upon the seven staring positions above 3200 cm^{-1} shown in Figure 7. Removal of any of the 10 bands worsens the goodness of fit to the observed spectra, while addition of more peaks in the fit produces unrealistic band positions relative to the obvious starting peak positions selected in Figure 7. We believe that the 10 H-positions determined in the neutron diffraction study are accounted for in the Raman spectra with some outstanding uncertainty regarding the number and positions of H_2O bending overtones.

Our diffraction and spectroscopic findings suggest that the stability of the structure of thaumasite under non-ambient conditions is mainly governed by the hydrogen-bonding geometry,

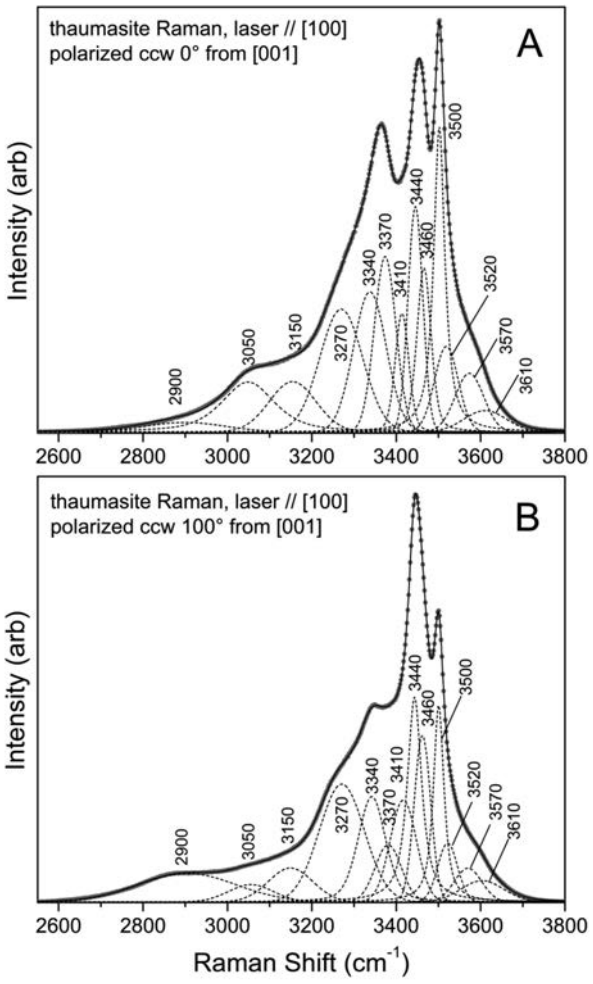

Figure 8. Deconvolution of the Raman spectra of thaumasite in the H_2O region showing fitted peaks associated with the ν_1 (O-H) stretching vibrations and H-O-H bending overtones. The largest variation of spectra are shown, between 0° (**a**) and 100° (**b**) polarized counterclockwise to [001] when the laser is directed along the [100] axis of the euhedral crystal.

because all of the major structural units [CO_3, SO_4, $Si(OH)_6$, Ca-polyhedra] are held together by hydrogen bonds. All the H bonds are stronger [i.e., d(O···O) shorter] at low temperature, but by different magnitudes (Table 5). The modest stability of thaumasite at high temperature, with the structure collapsing at $T \geq 420$ K (Martucci and Cruciani 2006), likely reflects the incapacity of the H-bonding scheme to be preserved at $T > 400$ K. Because low temperature stabilizes the thaumasite structure, pronounced sulfate attack of Portland cements observed in cold regions occurs likely in response to favorable nucleation and crystal growth of thaumasite under such conditions. Mitigation of thaumasite sulfate attack of cement needs to be developed for concrete structures, especially in cold regions and where sulfate-rich ground water is in contact with such structures or in waste-storage applications.

Acknowledgments

The authors thank the Institut Laue-Langevin, Grenoble, France, for the allocation of neutron beam time and the National Museum of Natural History, Smithsonian Institution, for the thaumasite sample. The access to major research facilities program for GJMcI is supported by the Commonwealth of Australia under the International Science Linkages program. S.D.J. acknowledges support from the U.S. National Science Foundation (EAR-0748707, CAREER), the Carnegie/DOE Alliance Center (CDAC), and the David and Lucile Packard Foundation. The Associate Editor (Lars Ehm), two anonymous reviewers, and the Technical Editor (Ron Peterson) are thanked for their constructive comments.

References cited

Barnett, S.J., Adam, C.D., and Jackson, A.R.W. (2000) Solid solutions between ettringite, $Ca_6Al_2(SO_4)_3(OH)_{12}\cdot 26H_2O$, and thaumasite $Ca_3SiSO_4CO_3(OH)_6\cdot 12H_2O$. Journal of Material Science, 35, 4109–4114.

Bensted, J. (1999) Thaumasite—background and nature in deterioration of cements, mortars and concretes. Cement and Concrete Composites, 21, 117–121.

Bickley, J.A. (1999) The repair of Arctic structures damaged by thaumasite. Cement and Concrete Composites, 21, 155–158.

Brough, A.R. and Atkinson, A. (2001) Micro-Raman spectroscopy of thaumasite. Cement and Concrete Research, 31, 421–424.

Busing, W.R. and Levy, H.A. (1964) The effect of thermal motion on the estimation of bond lengths from diffraction measurements. Acta Crystallographica, 17, 142–146.

Chiari, G. and Ferraris, G. (1982) The water molecules in crystalline hydrates studied by neutron diffraction. Acta Crystallographica, B38, 2331–2341.

Coppens, P., Leiserowitz, L., and Rabinovich, D. (1965) Calculation of absorption corrections for camera and diffractometer data. Acta Crystallographica, 18, 1035–1038.

Crammond, N.J. (1985) Thaumasite in failed cement mortars and renders from exposed brickwork. Cement Concrete Research, 15, 1039–1050.

Deb, S.K., Manghnani, M.H., Ross, K., Livingston, R.A., and Monteiro, P.J.M. (2003) Raman scattering and X-ray diffraction study of the thermal decomposition of an ettringite-group crystal. Physics and Chemistry of Minerals, 30, 31–38.

Edge, R.A. and Taylor, F.W. (1971) Crystal structure of thaumasite, $[Ca_3Si(OH)_6\cdot 12H_2O](SO_4)(CO_3)$. Acta Crystallographica, B27, 594–601.

Effenberger, H., Kirfel, A., Will, G., and Zobetz, E. (1983) A further refinement of the crystal structure of thaumasite, $Ca_3Si(OH)_6CO_3SO_4\cdot 12H_2O$. Neues Jahrbuch für Mineralogie Monatshefte, 2, 60–68.

Farrugia, L.J. (1999) WinGX suite for small-molecule single-crystal crystallography. Journal of Applied Crystallography, 32, 837–838.

Frost, D.J. and Fei, Y. (1998) Stability of phase D at high pressure and high temperature. Journal of Geophysical Research, 103, 7463–7474.

Gatta, G.D. and Boffa Ballaran, T. (2004) New insight into the crystal structure of orthorhombic edingtonite: evidence for a split Ba site. Mineralogical Magazine, 68, 167–175.

Gatta, G.D., Rotiroti, N., McIntyre, G.J., Guastoni, A., and Nestola, F. (2008) New insights into the crystal chemistry of epididymite and eudidymite from Malosa, Malawi: a single-crystal neutron diffraction study. American Mineralogist, 93, 1158–1165.

Grubessi, O., Mottana, A., and Paris, E. (1986) Thaumasite from the Tschwinning [N′Chwaning] mine, South Africa. Tschermaks Mineralogische und Petrographische Mitteilungen, 35, 149–156.

Hartshorn, S.A., Sharp, J.H., and Swamy, R.N. (1999) Thaumasite formation in Portland limestone cement pastes. Cement Concrete Research, 29, 1331–1340.

Hobbs, D.W. and Taylor, M.G. (2000) Nature of the thaumasite sulphate attack mechanism in field concrete. Cement and Concrete Research, 30, 529–533.

Jacobsen, S.D., Smyth, J.R., and Swope, R.J. (2003) Thermal expansion of hydrated six-coordinate silicon in thaumasite, $Ca_3Si(OH)_6(CO_3)(SO_4)\cdot 12H_2O$. Physics and Chemistry of Minerals, 30, 321–329.

Larson, A.C. (1967) Inclusion of secondary extinction in least-squares calculations. Acta Crystallographica, 23, 664–665.

Lehmann, M.S., Kuhs, W., McIntyre, G.J., Wilkinson, C., and Allibon, J. (1989) On the use of a small two-dimensional position-sensitive detector in neutron diffraction. Journal of Applied Crystallography, 22, 562–568.

Martucci, A. and Cruciani, G. (2006) In situ time resolved synchrotron powder diffraction study of thaumasite. Physics and Chemistry of Minerals, 33, 723–731.

Moore, A. and Taylor, H.F.W. (1970) Crystal structure of ettringite. Acta Crystallographica, B26, 386–393.

Reeder, R.J. (1983) Crystal chemistry of the rhombohedral carbonates. In R.J. Reeder, Ed., Carbonates: Mineralogy and Chemistry, 11, p. 1–47. Reviews in Mineralogy, Mineralogical Society of America, Chantilly, Virginia.

Renaudin, G., Sengi, R., Mentel, D., Nedelec, J.M., Leroux, F., and Taviot-Gueho, C. (2007) A Raman study of the sulfated cement hydrates: ettringite and monosulfoaluminate. Journal of Advanced Concrete Technology, 5, 299–312.

Sahu, S., Exline, D.L., and Nelson, M.P. (2002) Identification of thaumasite in concrete by Raman chemical imaging. Cement and Concrete Composites, 24, 347–350.

Santhanam, M., Cohen, M.D., and Olek, J. (2001) Sulfate attack research—wither now? Cement and Concrete Research, 31, 845–851.

Sears, V.F. (1986) Neutron scattering lengths and cross-sections. In K. Sköld and

D.L. Price, Eds., Neutron Scattering, Methods of Experimental Physics, 23A, p. 521–550. Academic Press, New York.
Sheldrick, G.M. (2007) A short history of SHELX. Acta Crystallographica, A64, 112–122.
Steiner, T. (1998) Opening and narrowing of the water H-O-H angle by hydrogen-bonding effects: Re-inspection of neutron diffraction data. Acta Crystallographica, B54, 464–470.
Thomas, M.D.A., Rogers, C.A., and Bleszynski, R.F. (2003) Occurrences of thaumasite in laboratory and field concrete. Cement and Concrete Composites, 25, 1045–1050.
Wilkinson, C., Khamis, H.W., Stansfield, R.F.D., and McIntyre, G.J. (1988) Integration of single-crystal reflections using area multidetectors. Journal of Applied Crystallography, 21, 471–478.
Yang, H., Prewitt, C.T., and Frost, D.J. (1997) Crystal structure of the dense hydrous magnesium silicate, phase D. American Mineralogist, 82, 651–654.
Zemann, J. (1981) Zur Stereochemie der Karbonate. Fortschritte der Mineralogie, 59, 95–116.
Zemann, J. and Zobetz, E. (1981) Do the carbonate groups in thaumasite have anomalously large deviations from coplanarity? Kristallografija, 26, 1215–1217.
Zhang, F.C., Ma, B.G., Yin, G., Wu, Y.Y., and Zhu, Y.C. (2009) Preparation and performance of sulfate resistance cement-based material. Key Engineering Materials, 400, 195–201.

Manuscript received November 23, 2011
Manuscript accepted April 3, 2012
Manuscript handled by Lars Ehm